Evaluation of Microstructure, Mechanical Properties and Corrosion Resistance of Friction Stir-Welded Aluminum and Magnesium Dissimilar Alloys

Jagesvar Verma, Ravindra V. Taiwade, Sanjay G. Sapate, Awanikumar P. Patil, and Ashwinkumar S. Dhoble

Microstructure, mechanical properties and corrosion resistance of dissimilar friction stir-welded aluminum and magnesium alloys were investigated by applying three different rotational speeds at two different travel speeds. Sound joints were obtained in all the conditions. The microstructure was examined by an optical and scanning electron microscope, whereas localized chemical information was studied by energy-dispersive spectroscopy. Stir zone microstructure showed mixed bands of Al and Mg with coarse and fine equiaxed grains. Grain size of stir zone reduced compared to base metals, indicated by dynamic recrystallization. More Al patches were observed in the stir zone as rotational speed increased. X-ray diffraction showed the presence of intermetallics in the stir zone. Higher tensile strength and hardness were obtained at a high rotational speed corresponding to low travel speed. Tensile fractured surface indicated brittle nature of joints. Dissimilar friction stir weld joints showed different behaviors in different corrosive environments, and better corrosion resistance was observed at a high rotational speed corresponding to low travel speed (FW3) in a sulfuric and chloride environments. Increasing travel speed did not significantly affect on microstructure, mechanical properties and corrosion resistance as much as the rotational speed.

1. Introduction

Many industrial domains like aerospace, automobile and shipbuilding industries highly emphasize on the dissimilar joining of aluminum (Al) and magnesium (Mg) alloys because of their high strength, light weight, more damping capacity, electromagnetic shielding and recyclability (Ref 1, 2). But, the oxidation of upper surface, porosity, solidification cracking and intermetallic formation are the foremost problems associated to join these dissimilar alloys by conventional and non-conventional techniques (Ref 1, 3, 4). The corrosion performance of Al and Mg alloys has also been a major barrier to their growth in many structural applications, instead of their high stiffness/ weight ratio, high damping capacity, ease of machinability, weldability, castability and recyclability (Ref 1). However,

Jagesvar Verma, Department of Metallurgical and Materials Engineering, Visvesvaraya National Institute of Technology (VNIT), South Ambazari Road, Nagpur, Maharashtra 440 010, India and School of Mechanical Engineering, Lovely Professional University (LPU), Phagwara, Punjab 144411, India; **Ravindra V. Taiwade, Sanjay G. Sapate,** and **Awanikumar P. Patil**, Department of Metallurgical and Materials Engineering, Visvesvaraya National Institute of Technology (VNIT), South Ambazari Road, Nagpur, Maharashtra 440 010, India; and **Ashwinkumar S. Dhoble**, Department of Mechanical Engineering, Visvesvaraya National Institute of Technology (VNIT), South Ambazari Road, Nagpur, Maharashtra 440 010, India. Contact e-mails: jageshwarverma28@gmail.com, rvtaiwadevnit@gmail.com, sgsapate@mme.vnit.ac.in, appatil14@gmail.com, asdhoble71@gmail.com.

friction stir welding (FSW) is one of the attractive advanced solid-state welding technique used to join similar and dissimilar ferrous and non-ferrous metals without any defects (Ref 4, 5). Friction stir welding can avoid most of the problems allied with dissimilar non-ferrous metal joining by fusion welding processes (Ref 6, 7). The only problem which associated with FSW is the formation of intermetallics (IMCs). Since the dissimilar welded joints of Al and Mg alloys are prone to corrosion in many aggressive environments due to the lower potential of Mg alloy and the formation of IMCs (Ref 1), the life prediction of dissimilar welded joint is also prime importance. It was reported (Ref 1) that the Al shows better corrosion resistance, especially in chloride environment than that of Mg. However, welding parameters are the factors which control IMCs formation and also help to improve the corrosion resistance (Ref 8). In most research, it was found that the higher rotational speeds caused thicker IMCs because of the increased heat input created by friction between the tool shoulder and workpiece (Ref 8). Liu et al. (Ref 9) stated that the high rotational speeds can influence the composition of IMC layers and higher welding speeds reduce the IMC thickness because of the shortening of the high-temperature period. Mofid et al. (Ref 10) carried out FSW of Al and Mg alloys in air and under water to see the cooling effect at a rotation speed of 300 rpm and traverse speed of 50 mm/min and reported the use of submerged friction stir welding (SFSW) under water as an alternative and improved method for creating fine-grained welds, which alleviate the formation of intermetallic phases. Authors concluded that the brittle compounds such as Al_3Mg_2, $Al_{12}Mg_{17}$ and Al_2Mg_3 appeared in the FSW by using an air media, which are the main reason for the formation of the weld crack, whereas the much lower amount of intermetallic compounds were formed in SFSW and weld crack has been avoided due to the temperature difference. J. Mohammadi et al. (Ref 11) demonstrated lap FSW joints between Mg-AZ31B and

Al-AA6061 dissimilar alloy sheets, which were made at various tool rotation (560-1400 rpm) and travel speeds (16-40 mm/min). Authors reported that the most of the joints were free of defects or cracks, except samples welded using a tool rotation speed of 560 mm/min and travel speed of 16 mm/min, in which a cavity defect was formed in the joint due to insufficient heat input. Jin et al. (Ref 12) demonstrated FSW (2-mm-thick plate) of Al-AA6061-T6 and Mg-AZ31B, performed at 1200 rpm and 101.6 mm/min by positioning Al-AA6061-T6 on retreating side and Mg-AZ31B on advancing side by taking the tool offset toward Mg alloy. In this case, the defect-free weld was obtained and the finer grains of Al-AA6061 were reported in the stir zone (SZ). Padmanaban et al. (Ref 13) investigated the effect of FSW process parameters on a mechanical property (tensile strength) of friction stir-welded AZ31B alloy by applying 1000-2000 rpm rotational speed and 0.37-2.25 mm/s welding speed. The authors reported that the joint produced with 1600 rpm/0.67 mm/s (rotational speed/welding speed) showed higher tensile properties (208 MPa) compared to other conditions. Authors also observed some issues on higher and lower rotational speed and reported that the high rotational speed (2000 rpm) produces microvoids due to excessive release of stirred materials to the upper surface, which reduced the tensile properties (203 MPa), while lower rotational speed (1000 rpm) results in lack of stirring, and this is one of the reasons for lower tensile properties (187 MPa) of the joints. Somashekaran et al. (Ref 14) performed FSW of three different Mg alloys with Al-AA6061 and concluded that the welds were free from porosities and comprised of homogeneous, equiaxed, fine-grained complex intercalated microstructures with recrystallized lamellar-like shear band rich in either Al or Mg. Authors also reported the complex intercalated microstructures in the FSW zone, which contributed to the haphazard elevated readings in the weld zone microhardness, the unusual, erratic hardness spikes exhibiting hardness values as much as three times that of the base material hardness.

Firouzdar et al. (Ref 6) demonstrated the importance of heat generation depending on the positioning of Mg or Al plate during welding, and authors stated that the amount of heat generation was more when Al placed on advancing side. Moreover, reduction in heat input results in improved joint strength. Chang et al. (Ref 15) performed hybrid laser-FSW of Al-AA6061-T6 and Mg-AZ31B alloys with or without using Ni foil at the faying surfaces to reduce intermetallics formation and reported that in both the cases intermetallics were appeared, but reduction in tensile strength was observed in case of without Ni foil compared to Ni foil. Corrosion behavior of Al and Mg alloys (AZ31, AZ80 and AZ91D) was demonstrated by electrochemical and gravimetric tests in 3.5 wt.% NaCl at 25°C. The authors reported that the formation of intermetallic $Mg_{17}Al_{12}$ at the interface of Mg matrix, which accelerates corrosion attack due to the formation of galvanic couple. Finally, it was reported that AZ91D and AZ80 alloys revealed the highest corrosion resistance.

Instead of huge demand of Al and Mg alloys, the previous studies have been mainly focused on the formation of intermetallics during joining and its prevention by adopting different techniques, but the systematic investigations on rotational speed and travel speed and its effect on microstructural development, joint strength, mechanical properties and especially, corrosion behavior of aluminum and magnesium dissimilar joints, particularly, in chloride and sulfuric environments are scanty. Therefore, the authors try to mount up the lay foundation for practical use in the fabrication industries at optimized condition by adopting three different rotational and two different travel speeds and its behavior in different corrosive environments. The corrosion studies with these parameters on Al/Mg dissimilar weldments are scare.

2. Materials and Experimental Procedure

Aluminum and Mg alloy BM plates (3.6 mm thick) were taken for the study. The chemical composition of BMs is mentioned in Table 1. Friction stir welding was performed on the Al and Mg plates of dimensions $100 \times 100 \times 3.6$ (mm). Aluminum and Mg alloy plates were placed on the retreating side and advancing side, respectively, with an offset of 0.2 mm toward Mg with butt configuration. Welding carried out on HMT-FN2EV milling machine of 10 HP motor. The photographic images of setup and tool are shown in Fig. 1(a) and (d). The FSW tool details are mentioned in Table 2. Joints were prepared by employing three different rotational speeds (850, 950 and 1050 rpm) and two different travel speeds (25 and 35 mm/min), designated as FW1 (850 rpm/25 mm/min), FW2 (950 rpm/25 mm/min), FW3 (1050 rpm/25 mm/min), FW4 (850 rpm/35 mm/min), FW5 (950 rpm/35 mm/min) and FW6 (1050 rpm/35 mm/min).

The specimens for the metallographic study were cut along the transverse direction of the weld by using wire-cut electric discharge machine (EDM). The weld cross section was polished with silicon carbide abrasive papers of grit sizes 220, 320, 600, 1000, 1200 and 1500 followed by velvet cloth polishing with 0.75 μm alumina powders. After polishing Al and Mg sides of the specimens were etched with Picral (14 ml picric acid, 2 ml glacial acetic acid, 2 ml distilled water) and Keller's (95 ml distilled water, 2.5 ml HNO_3, 1.5 ml HCl, 1 ml HF) reagents for 10 and 40 s, respectively (Ref 16).

The weld cross sections (after etching) were observed under Olympus optical microscope and scanning electron microscope (SEM) JEOL 6380A, and also elemental analysis was performed with energy-dispersive spectroscopy (EDS) equipped with SEM. Phase identification of welded joints was carried out by XRD technique. The tensile specimen was cut in the transverse direction according to ASTM-E 8-04 standard (Ref 17). All the tensile tests were performed at a constant strain rate of 1 mm/min on INSTRON 4467 (30 kN capacity) tensile testing machine. Fractography was analyzed by SEM. Vickers microhardness test over the SZ in the diameter range of tool shoulder (18 mm) is performed on MITUTOYO microhardness tester with the load of 200 g for 10-s loading time.

The corrosion test was carried out by using potentiodynamic polarization measurement in a 0.5 M NaCl and 0.5 M H_2SO_4 solution at room temperature at a sweep rate of 1 mV/s, from the free corrosion potential to +0.2 V (SCE). Prior to each experiment, the specimens were grounded mechanically up to 1000 grit. Each test performed three times to confirm the reproducibility.

3. Result and Discussion

3.1 Microstructure

Sound joints were produced by various welding conditions, employing 18 mm diameter tool shoulder. The view of joints at the top surface is illustrated in Fig. 1(b), (c), (e), and (f).

Table 1 Chemical composition of base metals

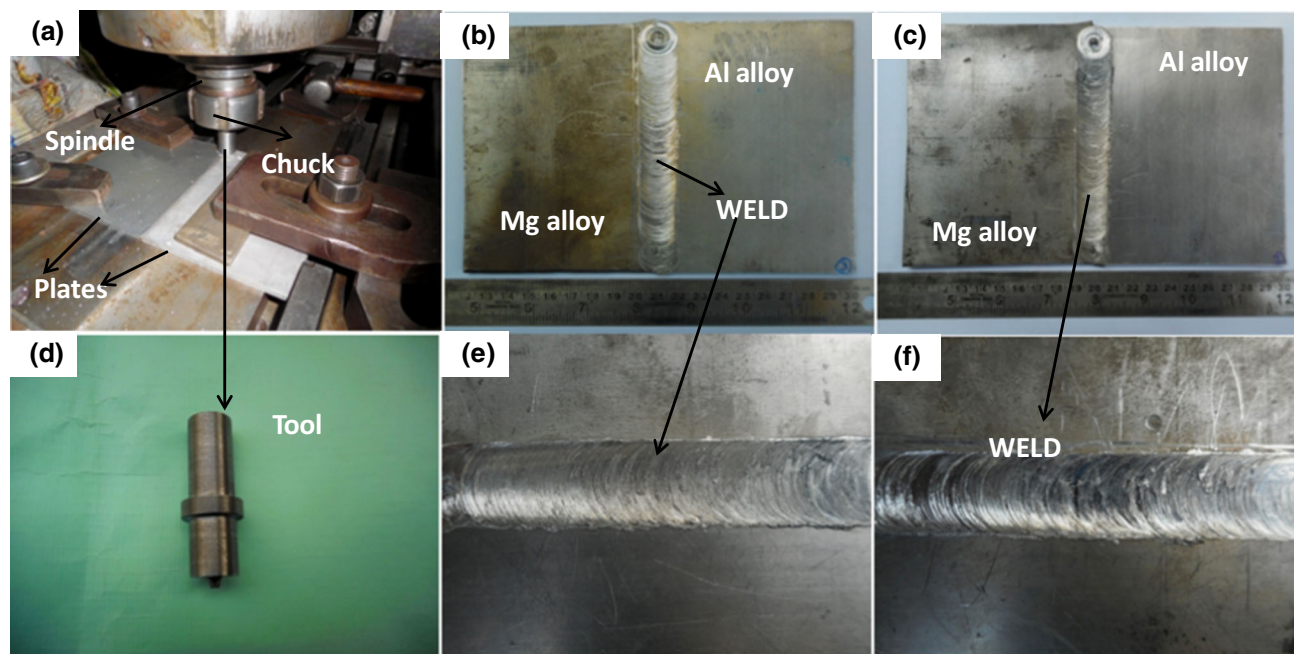|	Nominal chemical composition						
Materials	Mg	Al	Si	Cu	Fe	Zn	Mn
Mg-Z31B	Bal.	3.0	0.1	0.5	0.05	0.8	0.4
Al-A6061	0.95	Bal.	0.8	0.1	0.5	0.3	…

Fig. 1 Photographic views of welding setup, tool and weld joints (a) welding setup, (b) FW3 and (c) FW6 illustrated to welded joints, only FW3 and FW6 illustrated to represent other conditions (d) FSW tool, (e) and (f) showed enlarged view of welded joint

Table 2 FSW tool details

Tool material	H13
Shoulder diameter	18 mm
Tool pin profile	Taper pin
Root pin diameter	5 mm
Tip pin diameter	3 mm
Pin length	3.4 mm
Tool tilt angle	1.5°
Pin surface	Threaded groove

Optical micrograph of Al and Mg BMs is shown in Fig. 2. Large grains were observed in both the BMs. Figure 3(a) and (b), respectively, illustrates low magnification SEM macrograph of FS weld zone and enlarged view (SEM micrograph) of Al and Mg alloys distribution. Heavy intermixing was observed in SZ as illustrated in Fig. 3(a).

The optical micrographs of various locations in SZ at different welding conditions are shown in Fig. 4 and 5. Demarcation line (Fig. 6a-b) was observed between SZ and Al BM in all the joints. The existence of demarcation line in the interface may be due to discontinuity in materials flow (Ref 18, 19). Only FW1 and FW6 conditions are illustrated in Fig. 6(a) and (b) as a representative of all the conditions (due to similarity).

The micrograph (Fig. 4a) of condition FW1 (850 rpm/25 mm/min) showed a fine and coarse grains of Mg, which

indicated inhomogeneous deformation in the localized region caused to localized grain growth (Ref 20, 21), the measured average grain size (measured by optical microscope) was ∼4.9 μm. More Mg alloy was observed in SZ at this rotational speed compared to Al alloy, it was expected because Mg alloy was placed on the advancing side. However, the measured grain size (in FW1 condition) was much smaller than that of BMs grains (∼42 μm). Similarly, increasing the rotational speed at fixed travel speed (25 mm/min) from 850 (FW1) to 950 (FW2) and 1050 (FW3), the microstructure was slightly changed, more Al patches were observed with coarse equiaxed grains. It was reported (Ref 22) that the increasing rotational speed generated more frictional heat, which causes the formation of coarse equiaxed grains, the measured grain size was ∼5.3 μm in FW2 condition and ∼6.5 μm in FW3 condition. It was also noticed that the formation of intermetallic phases increased as rotational speed increased. But, the measured average particles size of intermetallics phase in FW1 (∼6.9 μm), FW2 (∼5.2 μm) and FW3 (∼4.5 μm) conditions were reduced as rotational speed increased. From the literature, it was reported (Ref 22) that the high rotational speed crushing the particles due to the high stirring action of a tool on the workpiece.

In condition, FW2 coarse equiaxed grains with an alternative lamellar band of Al and Mg alloy was observed as illustrated in Fig. 4(b). Further at high rotational speed (1050 rpm) FW3 condition, more amount of Al alloy was observed as shown in Fig. 4(c), some oxide layers was also
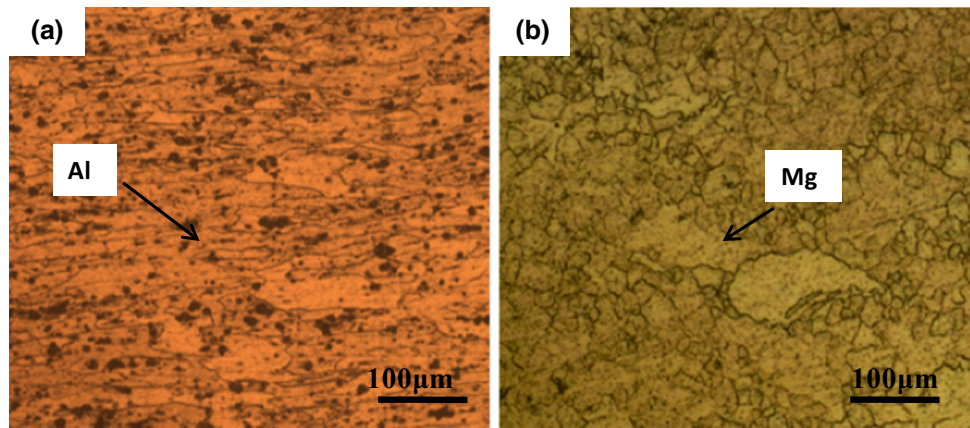
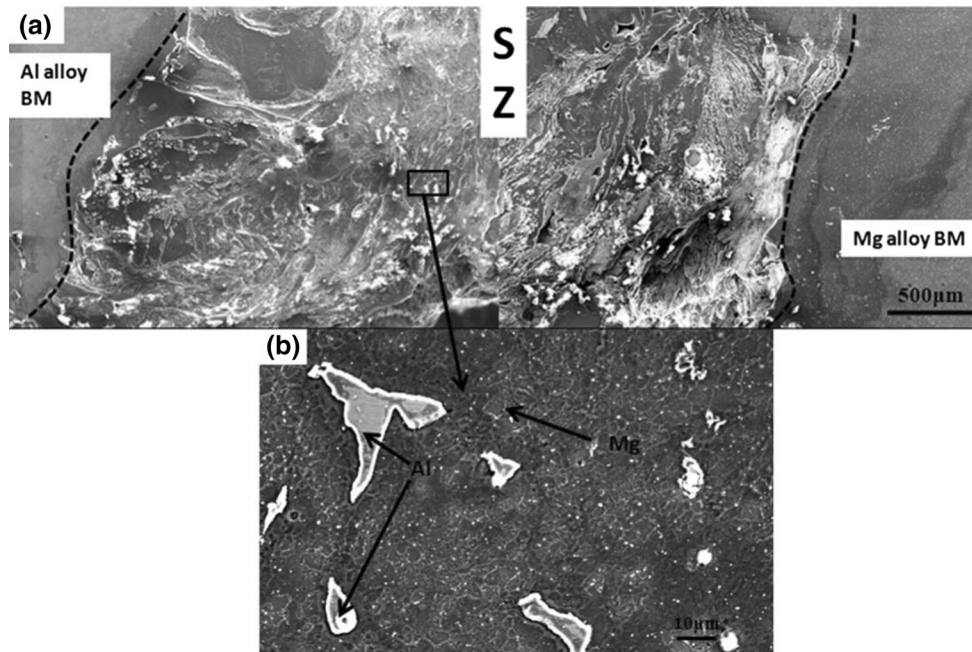**Fig. 2** Optical micrograph of BM (a) Al alloy BM, (b) Mg alloy BM

Fig. 3 SEM macrograph and micrograph of SZ (a) low magnification SEM micrograph of SZ (b) enlarged view of SZ to show the distribution of Al and Mg alloy. Note these represent all other conditions

noticed and it may be due to more frictional heat generation (Ref 13, 23). The increased amount of Al alloy in the SZ was due to more yield strength and flowability of Al than that of Mg (Ref 24). In all the conditions the SZ microstructures was comprised with intermingled lamellae band of Al and Mg alloy due to material agglomeration caused by helical vertical rotational flow of material created by tool action as reported by Gerlich (Ref 25).

On the other hand, for a fixed rotational speed (as mentioned above) and changing the travel speed from 25 mm/min to 35 mm/min did not change significantly the heat generation and further, the particles and grain size in condition FW4, FW5 and FW6. The measured grain size was ~ 4.6 μm (FW4), ~ 5.7 μm (FW5) and ~ 6.2 μm (FW6), which was very similar to previously mentioned condition. It was noticed that the increased travel speed caused to the formation of oxide layers and intermetallic phases. In Fig. 5(a), the microstructure obtained from FW4 condition showed intermingled band of

Al and Mg alloy very similar to FW1 condition. Similarly, more oxide layer formed in the case of FW5 and FW6 as shown in Fig. 5(b) and (c), respectively.

The intermetallic phases were predicted as $Al_{12}Mg_{17}$ and Al_3Mg_2 according to the Al-Mg binary phase diagram (Fig. 7a) and similarly reported by other researchers (Ref 15, 20, 21). Al_3Mg_2 intermetallic was observed (Fig. 7b) in SZ and Al alloy BM side due to the presence of more Al, as observed from Al-Mg binary diagram, whereas in SZ and toward Mg alloy interface side predominantly $Al_{12}Mg_{17}$ intermetallic phase was evident (Fig. 7c) which may be due to more amount of Mg composition. Scanning electron microscope attached with EDS analysis revealed the presence of intermetallic phases in all welding conditions, especially in the interface of Mg/Al BM and SZ as shown in Fig. 7. More intermetallics were evident in FW3 and FW6 conditions owing to more heat retention during welding (Ref 15, 20).
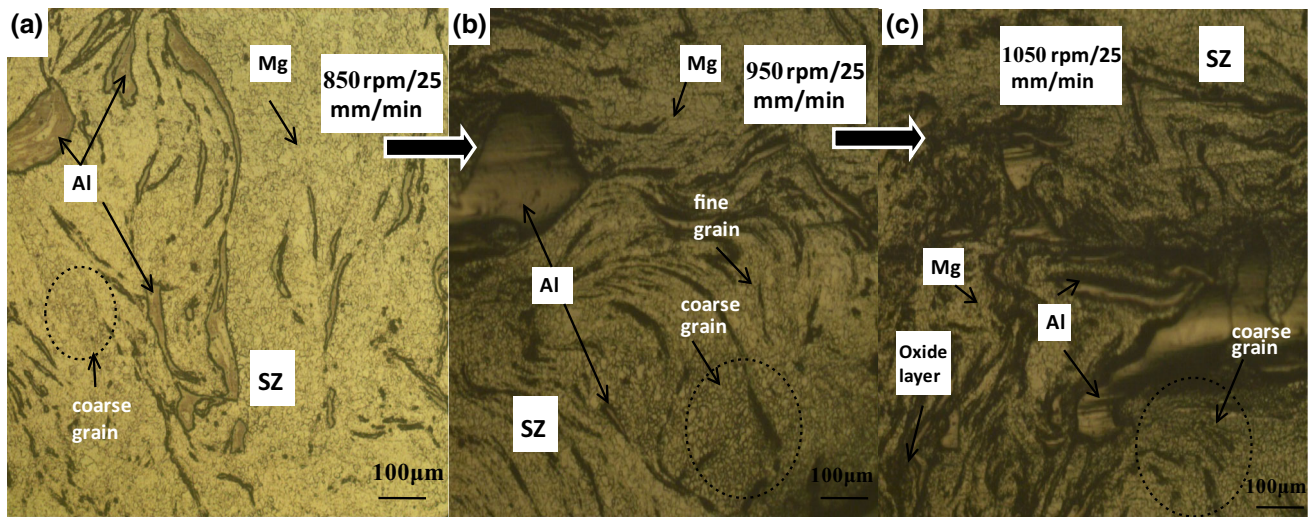
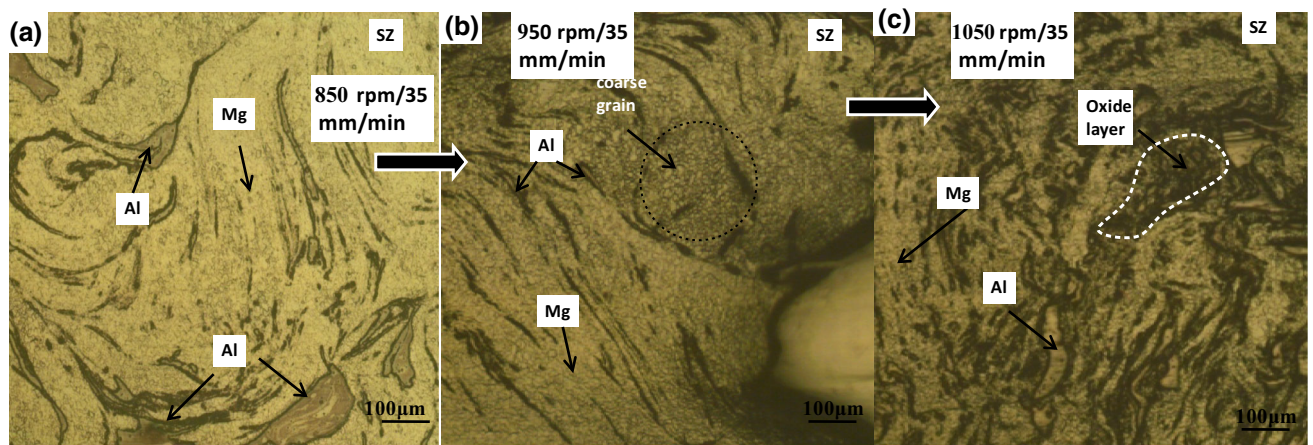**Fig. 4** Microstructures of SZ at different conditions (a) FW1, (b) FW2, (c) FW3

Fig. 5 Microstructures of SZ at different conditions (a) FW4, (b) FW5, (c) FW6
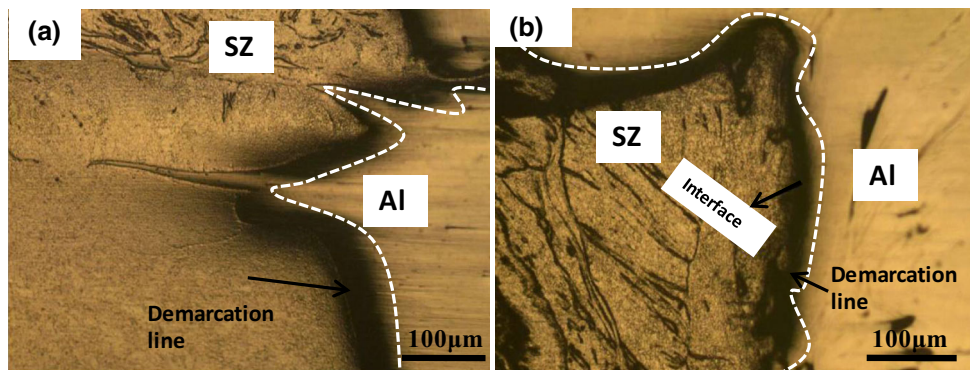

Fig. 6 Demarcation line at the interface represents all other conditions

The phase constituent in the SZ of Al and Mg dissimilar FS-welded joints was also analyzed by XRD to confirm the presence of intermetallics. The result of XRD analysis in Fig. 8 shows that besides Al and Mg solid solutions, Al_3Mg_2 and $Al_{12}Mg_{17}$ appeared in the friction stir weld, which is also the good agreement of Al-Mg binary diagram prediction.

3.2 Mechanical Properties

3.2.1 Tensile Test. The joint strength produced by all welding conditions is mentioned in Table 3. The failure occurred at the interface of Al and Mg alloy in SZ toward the advancing side. Flat facet fractured surface (Fig. 9) was
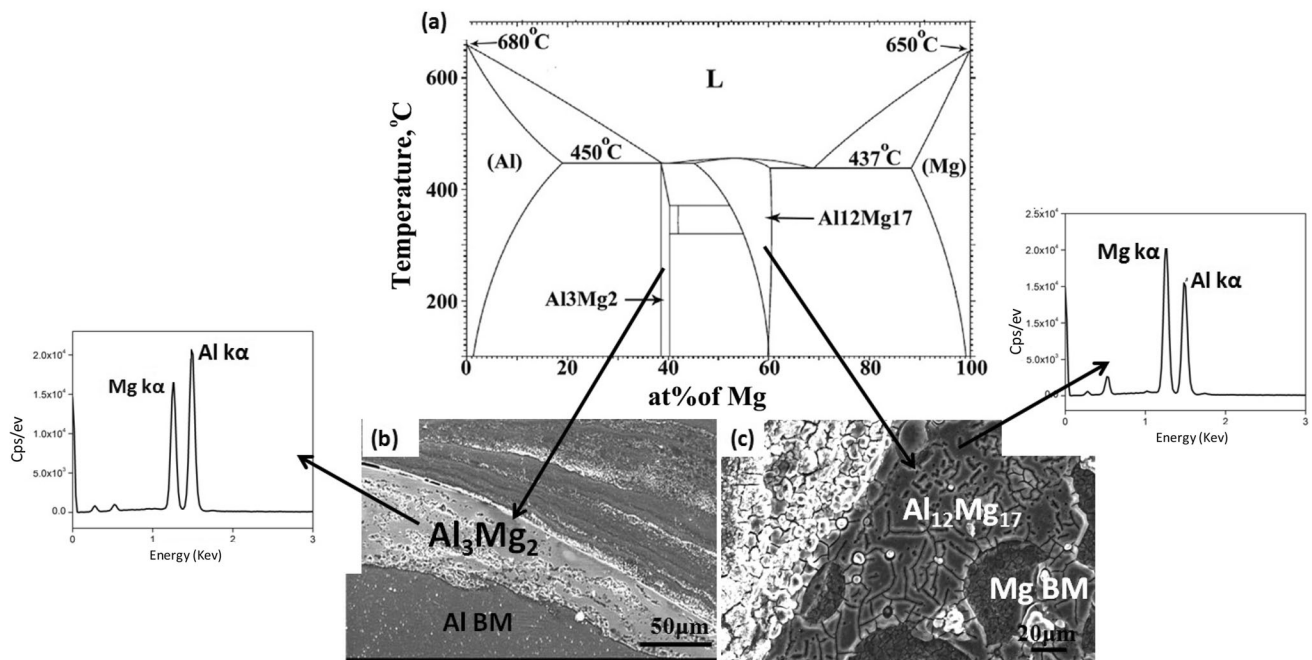
Fig. 7 Al-Mg binary phase diagram and intermetallics at the interface of BMs (a) Al-Mg binary phase diagram, (b) Al$_3$Mg$_2$ intermetallic at Al BM side and corresponding EDS point scan, (c) Al$_{12}$Mg$_{17}$ at Mg BM side and corresponding EDS point scan
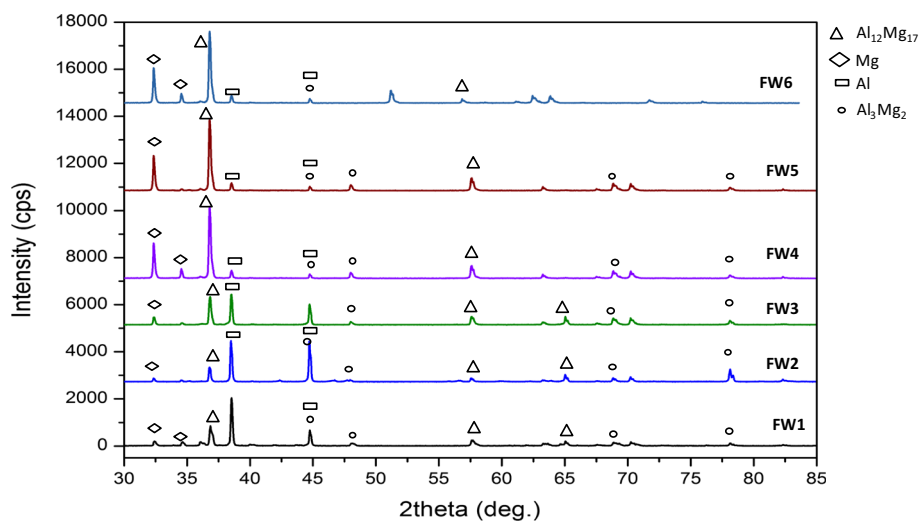

Fig. 8 X-ray diffraction patterns, showing the presence of Al, Mg and intermetallics

evident in all the conditions, which confirmed the existence of brittle nature of the welds. High rotational and low travel speed (FW3) showed higher tensile strength may be due to the formation and distribution of fine grains, intermetallics and more Al in the SZ. The presence of fine intermetallics increased the pinning effect, hence more energy required for dislocation movement as per Hall–Petch effect (Ref 19, 26, 27), which increased the tensile strength. The next high strength was measured in case of FW6. From the results, it was observed that the tensile strength reduced when increasing the travel speed from 25 to 35 mm/min. The wavy or river patterns along with tear ridge were observed through which the crack propagation occurred. River pattern (Fig. 9a, b) is present almost in all the fractured samples which were confirmed to be a brittle fracture.

3.2.2 Hardness. Vickers microhardness test was carried out on the transverse section of the weldments. For FW3 and FW6 condition, maximum hardness was measured in the transition region toward Mg alloy due to fine equiaxed grains and proper interlocking between Al and Mg phase (Ref 19, 27). While lower hardness was measured in the case of FW1 and FW4 than other conditions as reported in Table 3, FW2 and FW5 condition showed moderate hardness between FW1 and FW6. It was believed that more intermetallic formation and more intermixing of Al alloy with Mg alloy was the main cause to increase the hardness with high rotational speed, while in the case of low rotational speed Al alloy may not mix in more amount, resulting in lower hardness compared to high rotational speed. Moreover, high travel speed 32 mm/min did not much

Table 3 Mechanical properties of the FSW joints

Welding condition, rpm/mm/min	UTS, MPa	Average hardness (VHN)$_{0.2}$
850/25 (FW1)	78.52	155.8
950/25 (FW2)	89.32	159.2
1050/25 (FW3)	125.8	178.2
850/35 (FW4)	71.1	153.2
950/35 (FW5)	88.9	156.4
1050/35 (FW6)	111.6	167.6
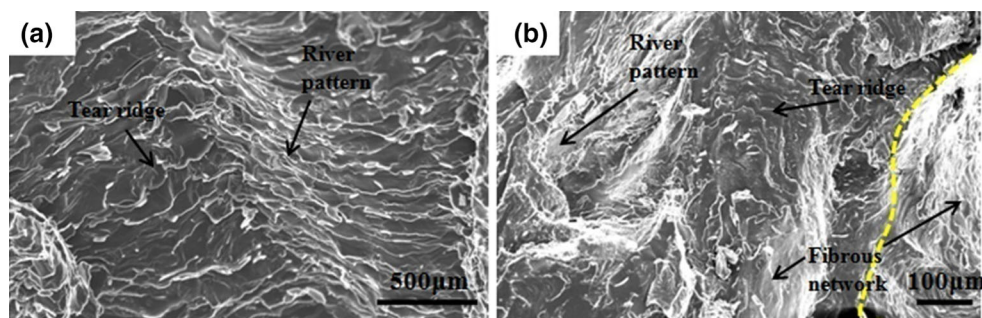
Fig. 9 Fractograph of fractured tensile samples FW3 and FW6 conditions represented all other conditions

Table 4 Electrochemical data of base metals and different joint conditions obtained from potentiodynamic polarization in 0.5 M NaCl solution

Welding conditions	Corrosion potential, E_{corr} (V vs. SCE)	Corrosion current density, I_{corr}, 10^{-5}, A/cm^2	Pitting potential, E_{pit}, V
Mg-AZ31B	−1.2	67	…
Al-AA6061	−0.62	1.3	−0.058
FW1	−1.06	2.1	−0.811
FW2	−0.99	33	−0.549
FW3	−0.80	1.2	−0.389
FW4	−1.1	1.6	−0.651
FW5	−0.91	21	−0.572
FW6	−0.83	16	−0.445

affect on hardness values compared to 25 mm/min. But in case of high rotational speed (1050 rpm), the significant variation was noticed as compared to low (850 rpm) and moderate (950 rpm) speed.

3.3 Corrosion Behavior

Potentiodynamic polarization curves of BMs and FS-welded samples at various conditions were measured with a scan rate of 1 mV$_{SCE}$/s after 1-h immersion in 0.5 M NaCl. E_{corr} (free corrosion potential) and i_{corr} (current density) are shown in Table 4, which are determined from Tafel extrapolation method, and curves are illustrated in Fig. 10. Table 4 also represents the E_{pit} values at various process parameters. It was found that the pitting resistance has improved at all parameters compared to the Mg alloy BM. Since Mg having lower potential and more reactive can easily dissolve in chloride environment (Ref 28). From the curves, much steeper anodic branch was noticed that indicated continuous dissolution of Mg alloy BM.

On the other hand, FW3 condition (higher rotational and lower travel speed) showed the wide passive range and higher

pitting potential (E_{pit} −0.389 V) compared to moderate and low-speed condition samples. From the results, it was believed that the pitting potentials did not change significantly with the travel speed and the pitting potential of FW6 (E_{pit} −0.445 V) was very similar as FW3. The i_{corr} values decreased with increase in rotational speed, thus indicating better resistance. The high rotational speed at lower travel speed increases the intermixing of Al and Mg alloys (Ref 1, 30), resulted in more presence of Al, Al oxide species and Mg$_{17}$Al$_{12}$ intermetallics with a formation of finer grains, as observed in FW3 and FW6 conditions. It was reported that the migration of Al^{+3} ions species through the passive layer resulted in thickening of the passive layer, are the main processes, which occur on the sample and its direct or indirect intervention improved corrosion resistance (Ref 31, 32). From the results, it was believed that FW3 has more corrosion resistance than FW6 due to finer grain, Al oxide and Mg$_{17}$Al$_{12}$ intermetallics than that of high travel speed 35 mm/min and high rotational speed (Ref 1, 29, 30). The E_{pit} values of FW1, FW2, FW4 and FW5 samples were −0.811, −0.549, −0.651 and −0.572 V, respectively, and highest pitting potential (E_{pit} −0.058) was measured in a case of Al BM.
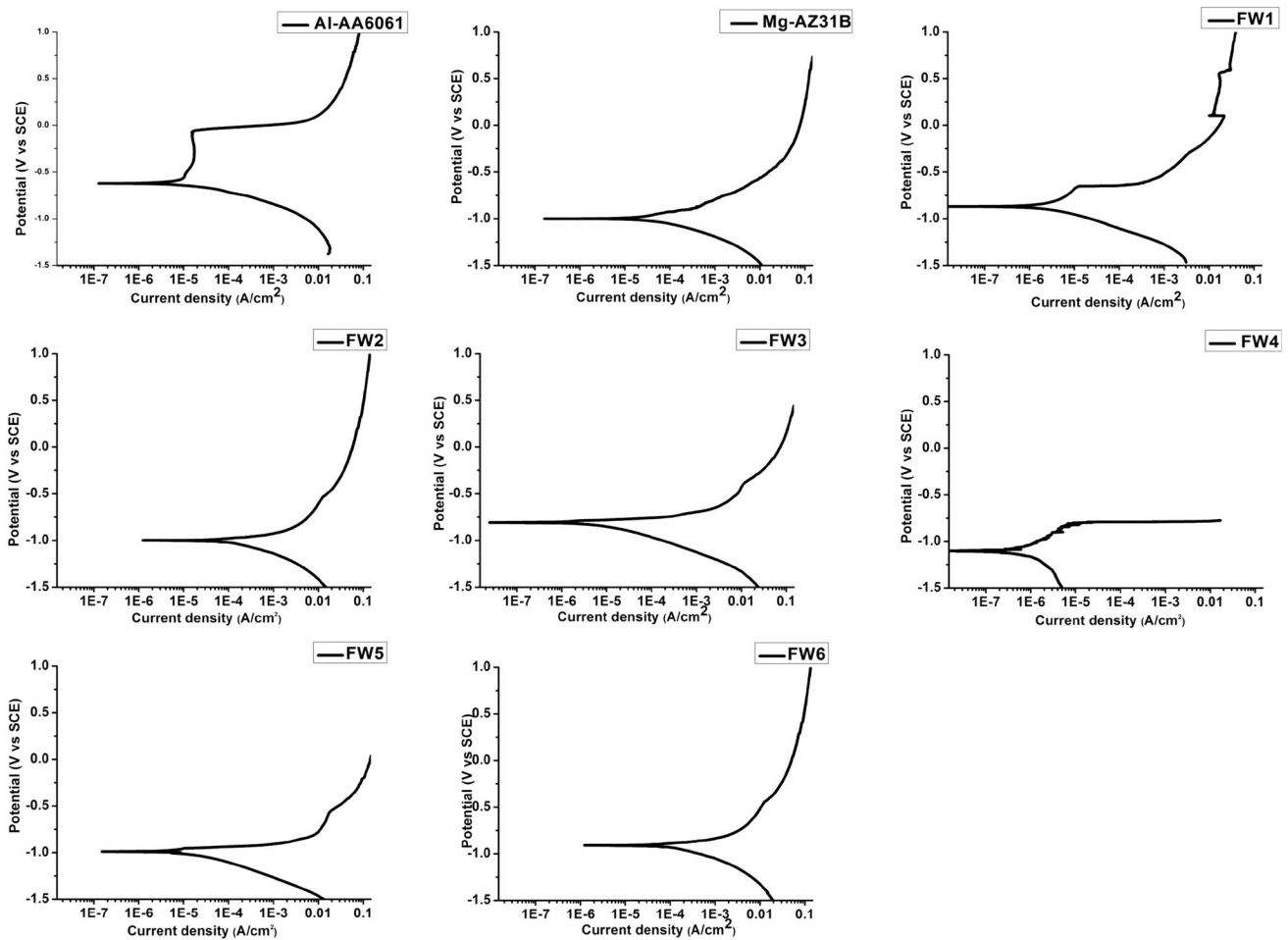
Fig. 10 Anodic polarization curves for base metals and all joint conditions in 0.5 M NaCl solution.

Table 5 Electrochemical data of base metals and different joint conditions obtained from potentiodynamic polarization studies in 0.5 M H₂SO₄ solution

Welding conditions	Corrosion potential, E_{corr} (V vs. SCE)	Corrosion current density, I_{corr}, 10^{-5}, A/cm²
Mg-AZ31B	−1.65	5266
Al-AA6061	−0.39	0.73
FW1	−1.37	3212
FW2	−0.68	212
FW3	−0.62	3.5
FW4	−1.29	2213
FW5	−0.71	112
FW6	−0.64	6.8

The FS-welded samples and BMs were also experienced in a sulfuric environment to get the overview of the electrochemical behavior of FS-welded samples at different parameters by using potentiodynamic polarization, the E_{corr} and i_{corr} are represented in Table 5, and curves are shown in Fig. 11. From the polarization curves, the quick dissolution of Mg alloy BM was observed compared to welded samples and Al alloy BM in H₂SO₄ solutions. Slightly lower corrosion current density and corrosion potential were observed in Mg alloy BM. However, dissolution of Al alloy BM was observed at higher potential. Aluminum generally shows passive behavior in aqueous/acidic solution due to the formation of a strong passive oxide film on the surface (Ref 33). The corrosion potential and the corrosion current density were different for BMs and welded samples. The FW3 (high rotational and low travel speed) condition showed improved potential (E_{corr} −0.390 V) than that of other welded conditions, and the fine-grained structure Al, Mg and intermetallics was reported to a formation of a more dense passive film helping to provide a better corrosion resistance. In FW 3 and FW6, both the conditions illustrated very similar polarization behavior in the sulfuric environment also, which again indicated that increasing travel speed did not have an influence on corrosion resistance in the sulfuric environment.
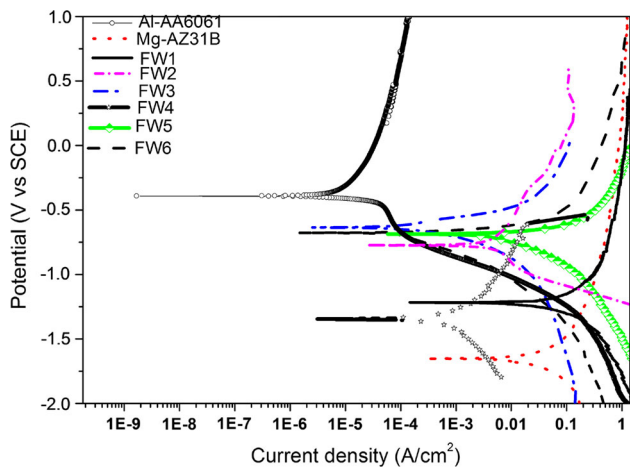
Fig. 11 Anodic polarization curves for base metals and all joint conditions in 0.5 M H_2SO_4 solution

Localized galvanic cells formed between the Al, Mg and intermetallics may be the reason for corrosion attack in FS-welded samples. Since the number of galvanic sites did not change with the variation in traverse speed, the corrosion resistance did not change with increasing travel speed (Ref 22). Further, the better corrosion resistance sequence in increasing series was Al-AA6061 > FW3 > FW6 > FW2 > FW5 ≫ FW1 > FW4 > Mg-AZ31B.

4. Conclusions

1. Defect-free sound joints were obtained in all the conditions.
2. Mixed microstructure of Al and Mg alloys was evident comprised with fine and coarse grains in all the welding conditions. Oxide layers and intermetallics appeared with increasing rotational speed.
3. Grain refinement was observed in the stir zone compared to base metals.
4. High rotational and low travel speed (FW3) showed higher strength and hardness due to presence of more Al alloy and fine $Al_{12}Mg_{17}$ and Al_3Mg_2 intermetallics.
5. Intermetallics formation in stir zone caused brittle fracture.
6. High rotational and low travel speed (FW3) showed improved corrosion resistance in chloride and sulfuric environments than that of high rotational and high travel speed.
7. All the joint conditions showed improved corrosion resistance compared to Mg alloy.

References

1. A. Pardo, M.C. Merino, A.E. Coy, R. Arrabal, F. Viejo, and E. Matykina, Corrosion Behavior of Magnesium/Aluminum Alloys in 3.5 wt% NaCl, *Corros. Sci.*, 2008, **50**, p 823–834
2. J.E. Gray and B. Luan, Protective Coatings on Magnesium and its Alloys—A Critical Review, *J. Alloys. Compd.*, 2002, **336**, p 88–113
3. M. Yamamoto, A. Gerlich, T.H. North, and K. Shinozaki, Cracking and Local Melting in Mg-Alloy and Al-Alloy During Friction Stir Spot Welding, *Weld. World*, 2013, **52**, p 38–46
4. M.A. Mofid and F.M. Ghaini, The Effect of Water Cooling During Dissimilar Friction Stir Welding of Al Alloy to Mg Alloy, *Mater. Des.*, 2012, **36**, p 161–167
5. Y.J. Kwon, I. Shigematsu, and N. Saito, Dissimilar Friction Stir Welding between Magnesium and Aluminum Alloys, *Mater. Lett.*, 2008, **62**, p 3827–3829
6. V. Firouzdor and S. Kou, Al-to-Mg Friction Stir Welding: Effect of Material Position, Travel Speed and Rotation Speed, *Metall. Mater. Trans. A Phys. Metall. Mater. Sci.*, 2010, **41**, p 2914–2935
7. D. Liu, H. Nishio, and K. Nakata, Anisotropic Property of Material Arrangement in Friction Stir Welding of Dissimilar Mg Alloys, *Mater. Des.*, 2011, **32**, p 4818–4824
8. M. Pourali, A. Abdollah-zadeh, T. Saeid, and F. Kargar, Influence of Welding Parameters on Intermetallic Compounds Formation in Dissimilar Steel/Aluminum Friction Stir Welds, *J. Alloy. Compd.*, 2017, doi:10.1016/j.jallcom.2017.04.272
9. X. Liu, S. Lan, and J. Ni, Analysis of Process Parameters Effects on Friction Stir Welding of Dissimilar Aluminum Alloy to Advanced High Strength Steel, *Mater. Des.*, 2014, **59**, p 50–62
10. M.A. Mofid, A. Abdollah-zadeh, and F. Malek Ghaini, The Effect of Water Cooling During Dissimilar Friction Stir Welding of Al Alloy to Mg Alloy, *Mater. Des.*, 2012, **36**, p 161–167
11. J. Mohammadi, Y. Behnamian, A. Mostafaei, H. Izadi, T. Saeid, A.H. Kokabi, and A.P. Gerlich, Friction Stir Welding Joint of Dissimilar Materials Between AZ31B Magnesium and 6061 Aluminum Alloys: Microstructure Studies and Mechanical Characterizations, *Mater. Charact.*, 2015, **101**, p 189–207
12. K. Lee and E. Kwon, Microstructure of Stir Zone in Dissimilar Friction Stir Welds of AA6061-T6 And AZ31 Alloy Sheets, *Trans. Nonferrous Met. Soc. China*, 2014, **24**, p 2374–2379
13. G. Padmanaban and V. Balasubramanian, An Experimental Investigation on Friction Stir Welding of AZ31B Magnesium Alloy, *Int. J. Adv. Manuf. Technol.*, 2010, **49**, p 111–121
14. A.C. Somasekharan and L.E. Murr, Microstructures in Friction-Stir Welded Dissimilar Magnesium Alloys and Magnesium Alloys to 6061-T6 Aluminum Alloy, *Mater. Charact.*, 2004, **52**, p 49–64
15. W.S. Chang, S.R. Rajesh, C.K. Chun, and H.J. Kim, Microstructure and Mechanical Properties of Hybrid Laser-Friction Stir Welding between AA6061-T6 Al Alloy and AZ31 Mg Alloy, *J. Mater. Sci. Technol.*, 2011, **27**, p 199–204
16. C.B. Jagadeesha, Dissimilar Friction Stir Welding between Aluminum Alloy and Magnesium Alloy at a Low Rotational Speed, *Mater. Sci. Eng., A*, 2014, **616**, p 55–62
17. ASTM E 8-04, *Standard Practice for Preparation Tension Testing of Metallic Materials,* Philadelphia, PA, USA, 2004
18. Y.H. Yin, N. Sun, T.H. North, and S.S. Hu, Hook Formation and Mechanical Properties in AZ31 Friction Stir Spot Welds, *J. Mater. Process. Technol.*, 2010, **210**, p 2062–2070
19. A. Kostka, R.S. Coelho, J.D. Santos, and A.R. Pyzalla, Microstructure of Friction Stir Welding of Aluminium Alloy to Magnesium Alloy, *Scripta Mater.*, 2009, **60**, p 953–956
20. M. Azizieh, A. Sadeghi Alavijeh, M. Abbasi, Z. Balak, and H.S. Kim, Mechanical Properties and Microstructural Evaluation of AA1100 to AZ31 Dissimilar Friction Stir Welds, *Mater. Chem. Phys.*, 2016, **170**, p 251–260
21. M. Jabbari and C.C. Tutum, Optimum rotation Speed for the Friction Stir Welding of Pure Copper, *ISRN Mater. Sci.*, 2013, doi:10.1155/2013/978031

22. K. Surekha, B.S. Murty, and K. Prasad Rao, Effect of Processing Parameters on the Corrosion Behaviour of Friction Stir Processed AA 2219 Aluminum Alloy, *Solid State Sci.*, 2009, **11**, p 907–917

23. P. Pourahmad and M. Abbasi, Materials Flow and Phase Transformation in Friction Stir Welding of Al 6013/Mg, *Trans. Nonferrous Met. Soc. China*, 2013, **23**, p 1253–1261

24. J. Yan, Z. Xu, Z. Li, L. Li, and S. Yang, Microstructure Characteristics and Performance of Dissimilar Welds between Magnesium Alloy and Aluminium, *Scripta Mater.*, 2005, **53**, p 585–589

25. A. Gerlich, P. Su, M. Yamamoto, and T.H. North, Material Flow and Intermixing During Dissimilar Friction Stir Welding, *Sci. Technol. Weld. Join.*, 2008, **13**, p 254–264

26. H.M. Rao, W. Yuan, and H. Badarinarayan, Effect of Process Parameters on Mechanical Properties of Friction Stir Spot Welded Magnesium to Aluminum Alloys, *Mater. Des.*, 2015, **66**, p 235–245

27. S.H.C. Park, Y.S. Sato, and H. Kokawa, Microstructural Evolution and its Effect on Hall-Petch Relationship in Friction Stir Welding of Thixomolded Mg Alloy AZ91D, *J. Mater. Sci.*, 2003, **38**, p 4379–4383

28. C. Liu, D.L. Chen, S. Bhole, X. Cao, and M. Jahazi, Polishing-Assisted Galvanic Corrosion in the Dissimilar Friction Stir Welded Joint of AZ31 Magnesium Alloy to 2024 Aluminum Alloy, *Mater. Charact.*, 2009, **60**, p 370–376

29. R.S. Mishra and Z.Y. Ma, Friction Stir Welding and Processing, *Mater. Sci. Eng., R*, 2005, **60**, p 1–78

30. G. Song, A. Atrens, X. Wu, and B. Zhang, Corrosion Behaviour of AZ10 AZ490 and AZ80 in Sodium Chloride, *Corros. Sci.*, 1998, **40**, p 1769–1791

31. K. Amini and F. Gharavi, Influence of Welding Speed on Corrosion Behaviour of Friction Stir Welded AA5086 Aluminium Alloy, *J. Cent. South Univ.*, 2016, doi:10.1007/s11771-016-3180-3

32. K. Jafarzadeh, T. Shahrabiand, and M.G. Hosseini, EIS Study on Pitting Corrosion of AA5083-H321 Aluminum-Magnesium Alloy in Stagnant 3.5% NaCl Solution, *J. Mater. Sci. Technol.*, 2008, **24**, p 215–219

33. D. Mercier, M. Herinx, and M.G. Barthés-Labrousse, Influence of 1,2-Diaminoethane on the Mechanism of Aluminium Corrosion in Sulphuric Acid Solutions, *Corros. Sci.*, 2010, **52**, p 3405–3412